Enthalpy Distributions of Laser Driven
High Enthalpy Wind Tunnel

Makoto Matsui[1], Koji Shinmi[2]
The University of Tokyo, Bunkyo, Tokyo, 113-8656, JAPAN

Kimiya Komurasaki[3]
The University of Tokyo, Kashiwa, Chiba, 277-8561, JAPAN

and

Yoshihiro Arakawa[4]
The University of Tokyo, Bunkyo, Tokyo, 113-8656, JAPAN

A 2 kW class laser driven plasma wind tunnel was developed as a high speed and high density atomic oxygen generator. Using argon and oxygen as working gases, laser sustained plasma (LSP) was successfully produced in the plenum pressure range from 0.30 MPa to 0.95 MPa, and then the LSP was expanded to the vacuum chamber through the convergent-divergent nozzle. Next, plume characteristics were evaluated by Pitot probe and laser absorption spectroscopy. As a result, specific enthalpy distributions were found to have flat region of 3.8 MJ/kg to 4.8 MJ/kg at the radial position less than 3 mm.

Nomenclature

C_p	=	specific heat at constant pressure
c	=	velocity of light
d	=	distance between LSP and throat
f	=	flux density
h_0	=	total specific enthalpy
h_{chem}	=	chemical potential
h_w	=	specific enthalpy at the wall
I	=	probe laser intensity
I_0	=	incident probe laser intensity
K	=	integrated absorption coefficient
K_i	=	integrated absorption coefficient
k	=	absorption coefficient
k_B	=	Boltzmann constant
M	=	Mach number
M_i	=	molecular weight
m	=	mass of absorber
n	=	number density
n_O	=	number desnity of atomic oxygen
P	=	CO_2 laser power
p_{amb}	=	ambient pressure
p_{Pitot}	=	Pitot pressure
p_{plenum}	=	plenum pressure

---

[1] JSPS research fellow, Department of Aeronautics and Astronautics, 7-3-1 Hongo, Member AIAA.
[2] Graduate student, Department of Aeronautics and Astronautics, 7-3-1 Hongo.
[3] Associate Professor, Department of Advanced Energy, 5-1-5 Kashiwanoha, Kashiwa, Member AIAA.
[4] Professor, Department of Aeronautics and Astronautics, 7-3-1 Hongo, Member AIAA.

p_s	=	stagnation pressure
p^*	=	throat pressure
$\dot{q}$	=	heat flux
r	=	radial position
r_N	=	real leading edge radius
R	=	plume radius
R_{eff}	=	effective leading edge radius
T	=	translational temperature
T^*	=	throat temperature
u	=	flow velocity
u^*	=	flow velocity at the throat (sonic speed)
x	=	position in the laser path
y	=	distance between the flow axis and the laser path
z	=	distance from the nozzle exit
ν	=	laser frequency
ν_0	=	center absorption frequency
ν_{shift}	=	Doppler shift
$\Delta\nu_D$	=	Doppler width
θ	=	incident laser beam angle to the flow
γ	=	specific heat ratio

I. Introduction

Development of thermal protection systems (TPS) requires the simulation of entry and re-entry conditions at ground test facilities. Arc-heaters are widely used to generate such high enthalpy flows because of their long operational time, simple structure and ease of maintenance. [1–4] However, surface catalytic effects and active and passive oxidation of TPS materials have been recognized as important issues [5–8]; erosion of their electrodes poses an important obstacle because polluted flows make it difficult to evaluate chemical reaction rates in front of TPS surfaces.

Then, inductively coupled plasma (ICP) generators have garnered much attention. [9–12] Such generators have no electrode. They can produce an ideal test condition for TPS tests because they have no undesirable chemical reactions that result from erosion. Another advantage of such generators is that they can use even reactive gases such as carbon dioxide and oxygen because of their electrode-less heating. However, in ICP, plasma instability limits its operation pressure less than atmosphere. Thereby, high enthalpy flows with high plenum pressure are difficult to produce. [13, 14]

Therefore, laser sustained plasma (LSP) is one of alternative heating methods for high enthalpy flow generation. Since LSP is produced by focusing laser beam, it requires no-electrode and it is sustained even at the higher pressure than atmosphere. [15-16]

In this study, argon-oxygen LSP was produced by 2kW class continuous wave laser and it was expanded through the convergent-divergent nozzle to generate supersonic atomic oxygen flows. Then, plume characteristics were evaluated by Pitot probe and laser absorption spectroscopy (LAS). The measured flow properties were evaluated as a simulator for the re-entry and low earth orbit (LEO) environments.

II. Laser Sustained Plasma Generator

A. Concept of LSP generator

A conceptual figure of the LSP generator is shown in Fig. 1. A laser beam is focused into a plasma production chamber through a set of condensing lens and window. Once plasma is produced near a focal point, the plasma efficiently absorbs a beamed laser power through inverse bremsstrahlung radiation. This plasma is sustained where its propagation to the incident laser beam direction balances out the flow velocity. This is
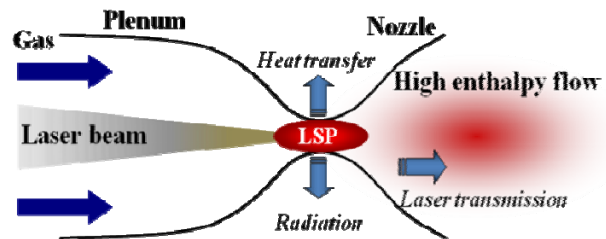

Fig.1 Conceptual figure of LSP generator.

called laser sustained plasma. The high-temperature LSP heats a working gas, and then the gas was expanded through a convergent-divergent nozzle to generate a high enthalpy flow.

In this generator, energy loss is composed of laser transmission and thermal loss. 17) The laser transmission is the unabsorbed laser power, which depends on the electron density and the volume of LSP. In thermal losses, the convective heat transfer to the chamber wall is usually small because the core of LSP does not attach directly to the wall and the cold flow surrounds the LSP. On the other hand, the radiative loss from the LSP increases with an increase in temperature of LSP. In this way, the energy efficiency of this generator depends on the energy balance in the energy transfer processes.

B. Experimental setup of LSP generator

A schematic of the LSP generator is shown in Fig. 2. The generator is composed of a laser induction window, a plasma-sustaining channel, and a convergent-divergent nozzle. The throat diameter is 1.0 mm and nozzle diameter is 20 mm. As a beam source, a continuous wave carbon dioxide laser (YB-L200B7T4, Matsushita Electric Industrial Co., Ltd.) was used. The wavelength is 10.6 μm. The maximum output power is 2 kW and the transverse mode of the laser beam is TEM10. The beam divergence is less than 2 mrad at the laser exit. The beam diameter of 20 mm was magnified by factor of 2.2 using a ZnSe beam expander, and the expanded beam was condensed into the generator through a ZnSe plano-convex lens. The focal length of the lens was 250 mm, corresponding to 7.4 in F-number which was defined as focal length normalized by beam diameter. This lens can move back to forth in the laser beam direction using a traverse stage.

A rod made of stainless steel (SUS304) was used as the source of the initial electron emission. After the ignition, the LSP was moved toward the nozzle throat by moving the focal lens position.

The generator is connected to a vacuum chamber. The chamber is 0.5 m in diameter and 1 m in length and it has two view windows enabling to diagnose an expanded flow. With two series of rotary vacuum pumps (ULVAC, VS1501;40 m3/h) and mechanical booster pumps (ULVAC, PRC012A; 500 m3/h), the ambient pressure can be kept under 106 Pa at the mass flow rate of argon 50 slm (1.5 g/s).
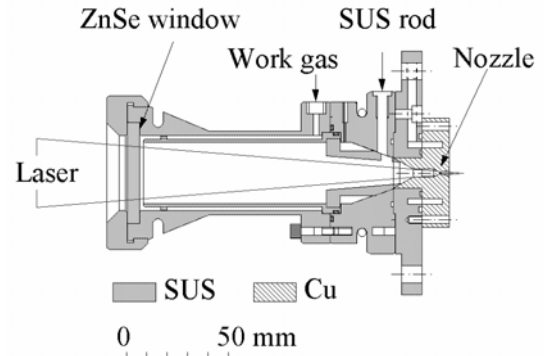

Fig.2 Schematics of LSP generator.

III. Measurement Methods

A. Pitot Probe Measurement

Mach number is estimated by the ratio of the Pitot pressure to the ambient pressure and stagnation pressure is estimated by the Pitot pressure and the Mach number using following Rayleigh supersonic Pitot formulae.

$$\frac{p_{\text{Pitot}}}{p_{\text{amb}}} = \left[\frac{(\gamma+1)M^2}{2}\right]^{\frac{\gamma}{\gamma-1}}\left[\frac{\gamma+1}{2\gamma M^2-(\gamma-1)}\right]^{\frac{1}{\gamma-1}} \tag{1}$$

$$\frac{p_{\text{Pitot}}}{p_{\text{s}}} = \left[\frac{(\gamma+1)M^2}{2+(\gamma-1)M^2}\right]^{\frac{\gamma}{\gamma-1}}\left[\frac{\gamma+1}{2\gamma M^2-(\gamma-1)}\right]^{\frac{1}{\gamma-1}} \tag{2}$$

A schematic of the Pitot probe developed at the University of Tokyo was shown in Fig.3. The probe made of cupper has a bore diameter of 2 mm and a probe outer diameter of 6 mm along the first 30 mm in length, and then it is covered by double tube cooling system whose outer diameter is 12 mm in order to protect the probe tip from melting. Pitot pressure was measured by a diaphragm gauge whose resolution was 0.13 Pa (DIAVAC Limited, FTR-1 and F-133k). The measurement point was 10 mm downstream from the
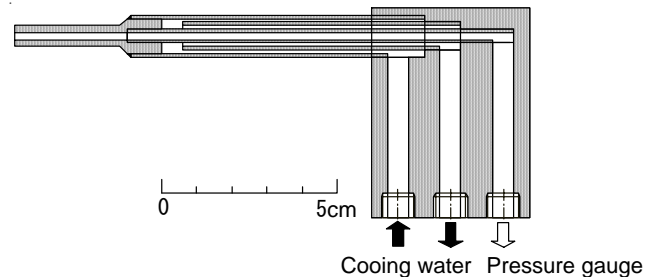

Fig.3 Schematics of UT mini probe.

nozzle exit.

B. Principle of Laser Absorption Spectroscopy

The translational temperature and the flow velocity were measured by a diode laser based LAS system developed at the University of Tokyo. [3,4]

The relationship between laser intensity and absorption coefficient is expressed by the Beer-Lambert law as

$$\frac{dI(\nu, y)}{dx} = -k(\nu, x, y) I(\nu, y) \tag{3}$$

Because the measured signals are composed of path-integrated absorption coefficient, the Abel inversion was applied to obtain the local absorption coefficient. When axisymmetric distributions of flow properties are assumed, the absorption coefficient in the radial coordinate is obtained as,

$$k(\nu, r) = \frac{1}{\pi} \int_r^R \frac{d\{\ln[(I/I_0(y,\nu))]\}/dy}{\sqrt{y^2 - r^2}} dy \tag{4}$$

The absorption coefficients are dependent on the frequency. Then the Abel inversion should be conducted frequency by frequency.

In our experimental conditions, Doppler broadening is several gigahertzes, which is two orders of magnitude greater than all other broadenings, including natural, pressure and Stark broadenings. The absorption profile is approximated as a Gaussian profile, expressed as

$$k(\nu, r) = \frac{2K(x)}{\Delta\nu_D} \sqrt{\frac{\ln 2}{\pi}} \exp\left[-\ln 2\left\{\frac{2(\nu - \nu_0 - \nu_{shift})}{\Delta\nu_D}\right\}^2\right] \tag{5}$$

The Doppler width is the full width at half maximum of the profile and is related to the temperature, expressed as

$$\Delta\nu_D = 2\nu_0 \sqrt{\frac{2k_B T}{mc^2} \ln 2} \tag{6}$$

The shift of the center absorption frequency by Doppler effect is related to the flow velocity, expressed as

$$\nu_{shift} = \frac{u\nu_0}{c} \sin\theta \tag{7}$$

The target line is the absorption from argon meta-stable state at 772.38 nm.

C. Measurement System of LAS

Figure 4 shows a schematic of the measurement system. A tunable diode-laser with an external cavity (Velocity Model 6300, New Focus, Inc.) was used as the laser oscillator. Its line width was less than 500 kHz. The laser frequency was scanned over the absorption line shape. The modulation frequency and width were 1 Hz and 30 GHz, respectively. The laser intensity, which was normalized by saturation intensity, was reduced less than 10-2 by neutral density filters; it was sufficiently small to avoid the influence of absorption saturation. (18 An optical isolator was used to prevent the reflected laser beam from returning into the external cavity. An etalon was used to calibrate relative frequency. Its free spectral range was 0.75 GHz. An argon glow discharge plasma tube (argon: 80 Pa, 250V) was used as a stationary plasma source to calibrate the laser frequency.

The probe beam was guided to the chamber window through an optical fiber. The fiber output was mounted on a one-dimensional traverse stage to scan the flow in the radial direction. The probe beam diameter was 1 mm at the chamber center. To reduce plasma emission, transmitted laser intensity was measured by a photo detector (DET110/M, Thorlabs,
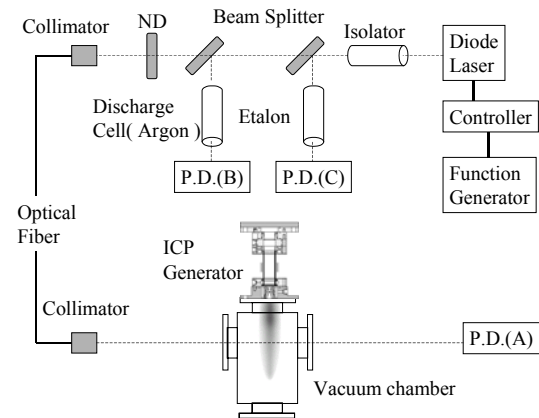

Fig.4 LAS measurement system.

Inc.) with a 2-mm pinhole and a band-pass filter whose full width at half maximum was 10 nm (FB770-10, Thorlabs, Inc.). A parabola mirror allowed scanning of the plume without synchronizing the detector position with the probe beam position. The signals were recorded using a digital oscilloscope with 16-bit resolution at the sampling rate of 10 kHz (DL1540; YOKOGAWA Co.). A measurement plane was 10 mm downstream from the nozzle exit and the incident laser beam angle was 5.0 degree.

IV. Results

A. Operation Conditions

Operation conditions are tabulated in Table 1. The LSP could be produced in the plenum pressure range from 0.30 MPa to 0.95 MPa. It should be remarked that at the plenum pressure of 0.95 MPa, the ZnSe window of 4 mm thickness and 50 mm in diameter was broken during the test. Then in this paper, the characterization test was not conducted at this condition. However, this doesn't mean the upper limit of the LSP production. The thicker window would enable to produce the LSP in the higher plenum pressure.

Figure 5 shows plume photos for the variation of the LSP position. Since the emission region of the plumes became larger with the closer position of the LSP to the nozzle throat, the LSP was optimized by moving a focal lens to maximize exhaust plume size. However, at the argon flow rate more than 40 slm, the position was not optimized. In our previous research, the LSP was found to move upstream with the increase in the plenum pressure.[17] Then, the focal point should be set downstream from the throat in order to move the LSP close to the throat. However, the relation between the focal length and the generator size disables to optimize the position. Thereby, in these conditions, the focal lens was set to the closest position to the generator window.

Table 1. Operation conditions.

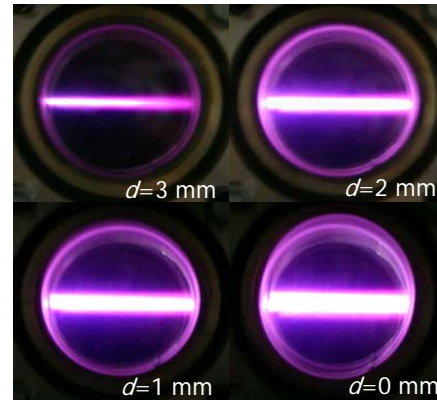| Properties	Value
Laser power, W	800
Argon, slm	10,20,30,40,50,(65)
Oxygen, slm	0.1
Plenum pressure, MPa	0.30-0.74 (0.95)
Ambient pressure, Pa	43-106 (122)

Fig.5 Plume photos for the variation of LSP position.

B. Pitot and stagnation pressure and Mach number

Figure 6 shows the Pitot pressure and estimated Mach number and stagnation pressure using Eqs. (1), (2). The Pitot pressure increases with the increase in the argon flow rate and has a maximum of 4.1 kPa at 30 slm. Then it slightly decreases in spite of the increase in the plenum pressure. This might be because the LSP would be produced upstream of the throat due to the unoptimized lens position and then the thermal loss to the wall increases, resulting in the lower increase in temperature and pressure.

Mach number has a maximum of 6.5 at 10 slm and then decreases to 5.0 with the argon mass flow rate. This might be also caused by the unoptimized LSP position.

Stagnation pressure was 45 kPa to 29 kPa. These values are less than 13 % of the plenum pressure. This significant pressure loss might by caused by the small throat diameter of 1 mm.
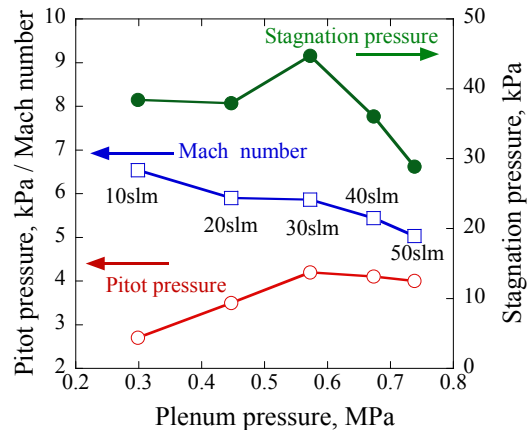

Fig.6 Pitot and stagnation pressure and Mach number.

C. Temperature and Velocity Distributions

Figure 7 shows typical transmitted laser intensity and etalon signals. The transmitted laser intensity fluctuated. The fluctuation of 270 Hz agrees with that of plasma emission. This might be caused by the LSP oscillation due to the fluctuation of the laser power. [19] In this study, the maximum absorption values in each fluctuation were extracted and a Gasuss distribution was fitted to the envelope of the maximum absorption absorbance as shown in Fig.8.

Figure 9 shows the deduce temperature distributions as a function of argon mass flow rate. The temperature has almost flat distributions of 280 K to 350 K in the radial region less than 5 mm.

Figure 10 shows the flow velocity distributions as a function of argon mass flow rate. The velocity has also flat distributions of 2650 m/s to 2890 m/s but its region is narrower than those of the temperature.
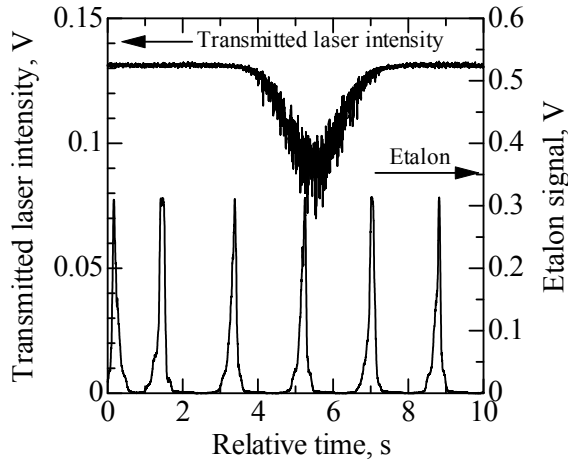

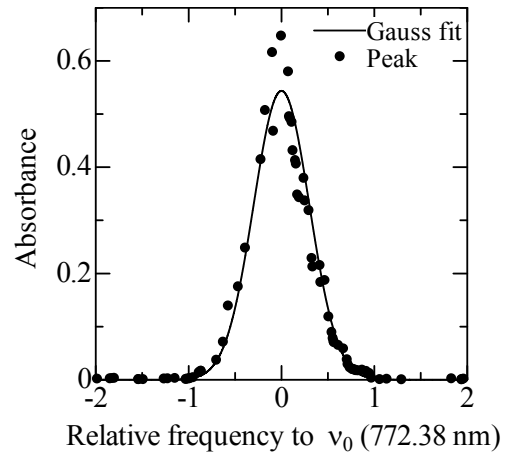**Fig.7 Typical transmitted laser intensity and etalon signals.**
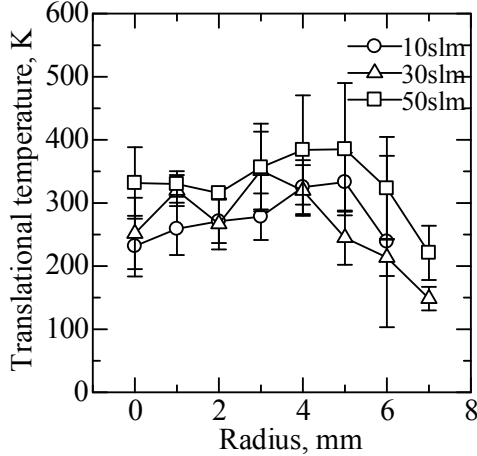

Fig.8 Absorbance and Gauss fit.
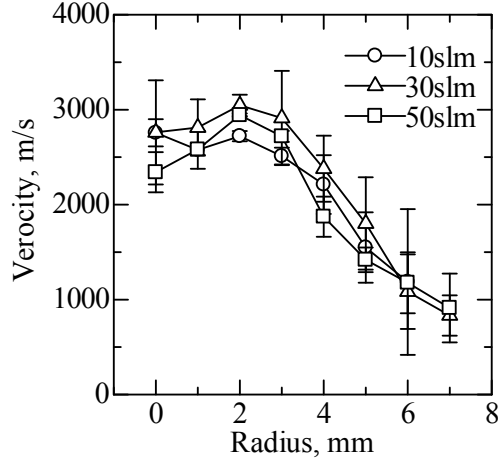

Fig.9 Temperature distributions.

Fig.10 Velocity distributions.

V. Discussions

A. Specific Enthalpy Distributions

The specific enthalpy and degree of dissociation in oxygen were estimated as follows. Assuming an isentropic expansion and chemically frozen flow through the nozzle, the total specific enthalpy at the throat and the plume is conserved expressed as

American Institute of Aeronautics and Astronautics

$$h_0 = \int_0^{T^*} C_p dT' + h_{chem} + \frac{1}{2}\gamma RT^* \qquad \text{(Throat)}$$

$$= \int_0^{T} C_p dT' + h_{chem} + \frac{1}{2}u^2 \qquad \text{(Plume)}$$

(8)

Here, the velocity at the throat is set to the sonic speed $u^* = \sqrt{\gamma RT^*}$ and the chemical potential is constant under the chemically frozen flow assumption.

Since the throat pressure estimated from the plenum pressure was higher than 0.15 MPa, the chemical composition in the plenum chamber of the flow was calculated assuming thermo-chemical equilibrium.

In the calculation, seven chemical species Ar, O_2, O, Ar^+, O_2^+, O^+ and e^-, and four chemical reactions $Ar \leftrightarrow Ar^+ + e^-$, $O_2 \leftrightarrow 2O$, $O \leftrightarrow O^+ + e^-$, $2O \leftrightarrow O_2^+ + e^-$ were considered. Their equilibrium constants were obtained from references 20 and 21. The volumetric gas mixture ratio argon and oxygen and the plenum pressure were set identical to the operation condition. The specific heat at the constant pressure was computed as the sum of the contributions of all species. Figure 11 shows typical calculated mole fraction and specific enthalpy as a function of the total temperature.

Using Eq. (8), the specific enthalpy and the degree of dissociation in oxygen were estimated. Figure 12 shows the estimated specific enthalpy distributions. The specific enthalpy has also flat region of 3.8 MJ/kg to 4.8 MJ/kg in the radial region less than 3 mm, where oxygen was found fully dissociated from Fig.11.
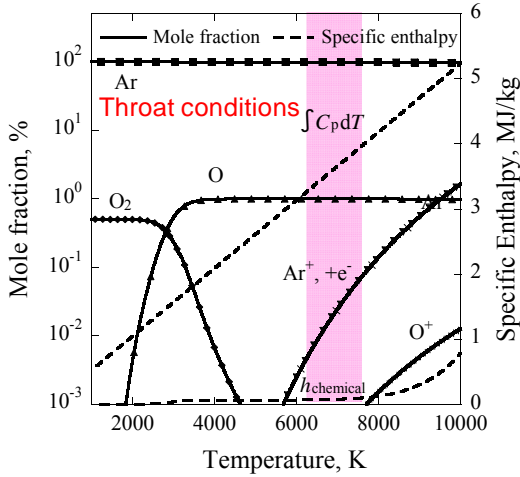

Fig.11 Typical calculated specific enthalpy and mole fractions using the thermo-chemical equilibrium assumption, p^*=0.22 MPa, volumetric mixture ratio Ar: O_2=20:0.1.
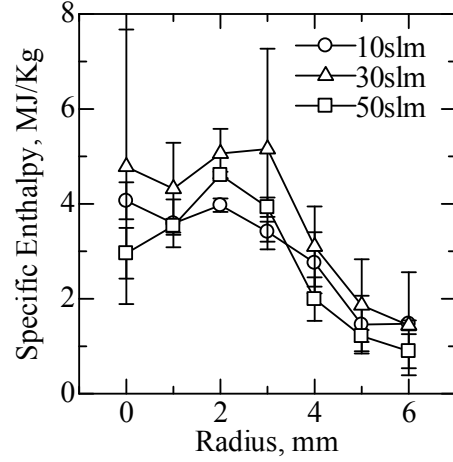

Fig.12 Specific enthalpy distributions.

B. Flow Validation as Re-entry Simulator

Heat flux is estimated from the measured specific enthalpy and stagnation pressure using Pope's equation, expressed as, [21]

$$\dot{q} = K\sqrt{\frac{p_s}{R_{eff}}}(h_0 - h_w)$$

(8)

Here, $R_{eff} = 2.9 r_N$ and r_N is set to the measured flat region of the specific enthalpy as 3mm, h_w is ignored and K_i is obtained from the reference 22 considering the mass fraction ratio.

Table 2 tabulates the estimated heat flux and those in various re-entry missions from LEO and superorbital. As seen in this figure, this wind tunnel flow covers heat flux conditions in re-entry missions with fully dissociated oxygen. Then, this wind tunnel is useful as a ground test facility for study in atomic

Table 2 Peak heat flux. [23]

Mission	Heat flux, kW/cm^2
HAYABUSA (CFD)	0.38+0.15 (conv+rad)
Apollo 11	0.326
Gemini	0.082
Space shuttle	0.022
This study	<0.54

oxygen behaviors in front of the TPS materials of re-entry missions.

C. Flow Validation as LEO Environment simulator

The flux density of the atomic oxygen was estimated as,

$$f = n_O u \tag{10}$$

Here, the number density of atomic oxygen was estimated by the equation of state $p_{amb}=nk_B T$ and the calculated mole fraction. Figure 14 shows estimated flux density of the atomic oxygen on the axis as a function of the plenum pressure. The maximum flux density was 2.2×10^{21} cm^{-2}s^{-1} at the plenum pressure of 0.30 MPa and then decreases with the increase in the plenum pressure.

Since in LEO, the flux density of the atomic oxygen is the order of 10^{15}cm^{-2}s^{-1}, this wind tunnel can simulate about two year exposure environment by only one min operation. However the flow velocity of 2.9 km/s is smaller than that of 7.8 km/s in LEO. Then, to increase the flow velocity, mixing with light atom is considered.

Approximately, the flow velocity is proportional to the square root of the total temperature and inverse molecular weight expressed as,

$$u \propto \sqrt{\frac{T_0}{M_i}} \tag{10}$$

Although the total temperature of the LSP depends on the core temperature of the LSP, which is the temperature at the maximum absorption coefficient of the inverse bremsstrahlung process, here it is assumed constant for simplicity.

Figure 14 shows estimated flow velocity as a function of oxygen, argon and helium mixture ratio. In pure oxygen case, the velocity is 4.7 km/s and still small. In case of oxygen and helium mixture, the mole fraction of helium is required more than 0.85 and the velocity is accelerated up to 9.5 km/s. However, the LSP generation without argon might be difficult to be produce because the ionization energy of helium (24.6 eV) is much higher than argon (15.8 eV). Then, the oxygen, helium and argon mixture case is considered. In this case, the mole fraction of the helium and argon should be larger than 0.9 and lower than 0.05, respectively.
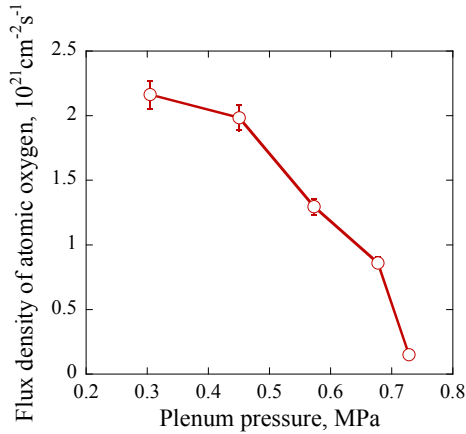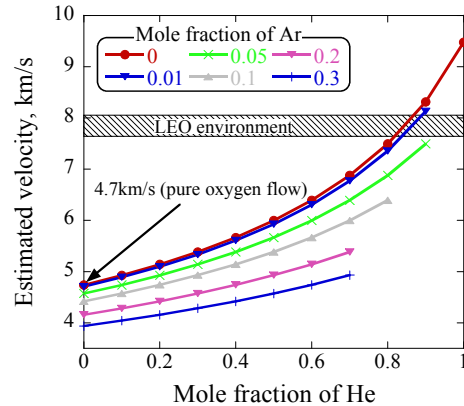

Fig.13 Atomic oxygen flux density.

Fig.14 Estimated flow velocity.

VI. Conclusion

A laser driven high enthalpy wind tunnel has been developed as a high speed and high density atomic oxygen generator. The flow characteristics were evaluated by Pitot probe and laser absorption spectroscopy. As a result, the Mach number, stagnation pressure and the specific enthalpy around the center were 5.0 to 6.5, 29 kPa to 45 kPa and 3.8 MJ/kg to 4.8 MJ/kg, respectively. This wind tunnel flows are found to be useful for study in the atomic oxygen behaviors in re-entry TPS materials. For the simulation of atomic oxygen environments in LEO, the flux density of atomic oxygen was enough to simulate two year exposure by one minute operation. But the flow velocity of 2.9 km/s was lower than actual velocity of 7.8 km/s. Then, to produce the actual flow velocity, mixing with helium is necessary.

Acknowledgments

References

[1]Birkan, M. A., "Arcjets and Arc Heaters: An Overview of Research Status and Needs," *Journal of Propulsion and Power*, Vol. 12, No. 6, 1996, pp. 1011–1017.

[2]Auweter-Kurtz, M., Kurtz, H. L., and Laure, S., "Plasma Generators for Re-Entry Simulation," *Journal of Propulsion and Power*, Vol. 12, No. 6, 1996, pp. 1053-1061.

[3]Bykova, N. G., Vasil'evskii, S. A., Gordeev, A. N., Kolesnikov, A. F., Pershin, I. S., and Yakushin, M. I., "Determination of the Effective Probabilities of Catalytic Reactions on the Surfaces on Heat Shield Materials in Dissociated Carbon Dioxide Flows," *Journal of Fluid Dynamics*, Vol. 32, No. 6, 1997, pp. 876-886.

[4]Balat, M., Flamant, G., Male, G., and Pichelin, G.., "Active to Passive Transition in the Oxidation of Silicon Carbide at High Temperature and Low Pressure in Molecular and Atomic Oxygen," J*ournal of Materials Science*, Vol. 27 1992, pp. 697-703.

[5]Kisa, M., Li, L., Yang, J., Minton, T., Stratton, W. G., Voyles, P., Chen, X., Benthem, K., and Pennyycook, S. J., "Homogeneous Silica Formed by the Oxidation of Si(100) in Hyperthermal Atomic Oxygen," *Journal of Spacecraft and Rockets*, Vol. 43, No. 2, 2006, pp.431-435.

[6]Fujimoto, L, Satoh, K., Shioya, T., Seki, N., and Fujita, K., "Degradation of Materials by High-Energy Atomic Oxygen," *JSME International Journal*, Series A, Vol. 46, No. 3, 2002, pp.283-289.

[7]Herdrich, G., Auweter-Kurtz, M.,"Development and Characterization of Inductively Heated Plasma Generator for Atmospheric Entry Simulations," AIAA Paper 04-2503, Jun. 2004.

[8]Matsui, M, Komurasaki, K., Herdrich, G., and Auweter-Kurtz, M. "Enthalpy Measurement in Inductively Heated Plasma Generator Flow by Laser Absorption Spectroscopy," *AIAA Journal*, Vol.43, No.9, 2005, pp. 2060-2064.

[9] Ito, I.., Ishida, K., Mizuno, M., Sumi, T., Fujita, K., Nagai, J., Murata, H. and Matsuzaki, T.: Heating Tests of TPS samples in 110kW ICP-heating wind tunnel, ISTS 2004-e-20

[10]Yamada, T., Fujita, K., Nonaka, S., Ishii, N., "Performance Characteristics of the Inductively-Coupled High Enthalpy Flow Generator with CO2 Gas," ISTS 2006-e-19.

[11] Plasma flow: http://www.vki.ac.be/research/themes/annualsurvey/2000/plasma_flows.pdf [cited 1 June 2008]

[12]Toyoda, K. Komurasaki, K., Arakawa, Y., "Continuous-wave laser thruster experiment," *Vacuum*, Vol.59, Issue 1, pp.63-72, 2000.

[13]Toyoda, K. Komurasaki, K., Arakawa, Y., "Thrust Performance of a CW Laser Thruster in Vacuum," *Vacuum*, Vol.65, Issue.3-4, pp.383-388, 2002.

[14]Inoue, T., Uehara, S., Komurasaki, K., Arakawa, Y., "Energy Conversion in a CW Laser Thurster," *Journal of the Japan Society for Aeronautical and Space Sciences*, Vol.54, No.627, pp.168-174, 2006.

[15]Inoue, T., Ijiri, T., Hosoda, S., Kojima, K., Uehara, S., Komurasaki, K., Arakawa, Y., "Oscillation phenomenon of laser-sustained plasma in a CW laser propulsion," *Vacuum*, Vol.73, No.3-4, pp.433-438, 2004.

[16]Matsui, M., Takayanagi, H., Oda, Y., Komurasaki, K., and Arakawa, Y., "Performance of arcjet-type atomic-oxygen generator by laser absorption spectroscopy and CFD analysis," *Vacuum*, Vol. 73, No. 3, 2004, pp. 341-346.

[17]Matsui, M., Ikemoto, T., Takayanagi, H., Komurasaki, K., Arakawa, Y.,"Generation of Highly Dissociated Oxygen Flows Using a Constrictor-Type Arc Heater," *Journal of Thermophysics and Heat Transfer*, Vol.21, No.1, 2007, pp. 247-249.

[18]Matsui, M., Ogawa, S., Komurasaki, K., Arakawa, Y., "Influence of Laser Intensity on Absorption Line Broadening in Laser Absorption Spectroscopy," *Journal of Applied Physics*, Vol. 100, 2006, 063102.

[19]Matsuzaki, R., "Quasi-One-Dimensional Aerodynamics with Chemnical Vibrational and Translational Nonequilibrium," *Transaction of Japan Society for Aeronautical and Space Science*, Vol. 30, No. 90, 1987, pp. 243-258.

[20]Guputa, R. N., Yos, J. M., Thompson, R. A., and Lee, K.-P., "A Review of Reaction Rates and Thermodynamic and Transport Properties for an 11-Species Air Model for Chemical and Thermal Nonequilibrium Calculations to 30000K," NASA RP-1232; L-16634; NAS 1.61:1232, 19900801, Aug, 1990.

[21]Pope, R. B., "Stagnation Point Convective heat Transfer in Frozen Boundary Layers," *AIAA Journal*, Vol. 6, No. 4, April 1968, pp.619-626.

[22] Zoby, E. V., "Empirical Stagnation-point Heat-transfer Relation in several Gas Mixtures at High Enthalpy Levels," NASA TN D-4799.

[23]Kubota, H., Suzuki, K., and Wtanuki, T., *Aerothermodynamics of Space Vehicles*, University of Tokyo Press, 2002.